Local environment of iodine dissolved as iodate in high-pressure aluminoborosilicate glasses: A I K-edge x-ray absorption spectroscopic study

Yann Morizet, Nicolas Trcera, Tomo Suzuki-Muresan, Sami Soudani, Emiliano Fonda, Michael Paris

Local environment of iodine dissolved as iodate in high-pressure aluminoborosilicate glasses: A I K-edge X-ray Absorption Spectroscopic study

Yann MORIZET[a*], Nicolas TRCERA[b], Tomo SUZUKI-MURESAN[c], Sami SOUDANI[a,d], Emiliano FONDA[b], Michael PARIS[d]

[a]Université de Nantes, Nantes Atlantique Universités, Laboratoire de Planétologie et Géodynamique de Nantes (LPG), UMR CNRS 6112, 2 rue de la Houssinière, 44322 Nantes Cedex, France

[b]Synchrotron SOLEIL, L'Orme des Merisiers, Saint Aubin, BP 48, F-91192 Gif-sur-Yvette Cedex, France

[c]SUBATECH (IMT Atlantique, CNRS/IN2P3, Université de Nantes), BP 20722, 44307 Nantes Cedex 3, France

[d]Université de Nantes, CNRS, Institut des Matériaux Jean Rouxel (IMN), 44000 Nantes, France

*Corresponding author: Yann Morizet

Postal address:

Laboratoire de Planétologie et Géodynamique (LPG), UMR-CNRS 6112, Université de Nantes.

2 rue de la Houssinière, 44322 Nantes Cedex (FRANCE)

phone: +33 (0) 2 5112 5491

fax: +33 (0) 2 5112 5268

*E-mail: yann.morizet@univ-nantes.fr

Abstract

The use of high-pressure synthesis conditions to produce I-bearing aluminoborosilicate represent a promising issue for the immobilization of ^{129}I radioisotope. Furthermore, iodine appears to be more solubilized in glasses under its iodate (I^{5+}) form rather than its iodide (I^-) form. Currently, the local atomic environment for iodine is poorly constrained for I^- and virtually unknown for I^{5+} or I^{7+}. We used I K-edge X-ray Absorption Spectroscopy conducted at 20 K for determining the local atomic environment of iodine dissolved as I^-, I^{5+}, I^{7+} in a series of aluminoborosilicate glasses. We determined that I^- is surrounded by either Na^+ or Ca^{2+} in agreement with previous works. The signal collected from EXAFS reveals that I^{5+} is surrounded invariably by three oxygen atoms forming a IO_3^- cluster charge compensated by Na^+ and/or Ca^{2+}. The I-O distance in iodate dissolved in glass is comparable to the I-O distance in crystalline compounds at ~1.8 Å. The distance to the second nearest neighbor (Na^+ or Ca^{2+}) is also constant at ~3.2 Å. This derived distance is identical to the distance between I^- and Na^+ or Ca^{2+} in the case of iodide local environment. For one sample containing iodate and periodate, the distinction between the local environment of I^{5+} and I^{7+} could not be made suggesting that both environments have comparable EXAFS signal.

I. INTRODUCTION

Nowadays, the nuclear energy is a part of energetic mix along with fossil fuels and renewable sources for energy consumption of industrialized countries[1 2 3]. However, on the contrary to fossil fuels, nuclear energy does not contribute to increase the greenhouse effect[3]; and on the contrary to renewable energy source (i.e. wind and solar) nuclear energy is continuous and not dependent on seasonality[4]. Although nuclear energy has several benefits, it actually produces radioactive wastes that need to be handled in a durable and safe manner[5]. From the many radioactive isotopes produced by nuclear plant activities, 129-iodine (^{129}I) represents a major troublesome element, as it is highly mobile in the environment, has a long half-life (15.7 My) and can be assimilated by the human organism[6 7 8 9 10 11 12 13]. Furthermore, ^{129}I does not actually benefit from a fully adequate specific matrix to immobilize this radiotoxic isotope in a permanent manner in natural geological repository site.

Many efforts have been conducted in the last decade to propose specific matrices for the ^{129}I immobilization such as glass (e.g. phosphate-based, silver-based, borosilicate-based)[14 15 16 17], crystalline phases[18 19 20] or glass ceramics[21 22 23]. Borosilicate glasses are of interest as it has a good chemical and mechanical durability[24 25 26 27]. However, because borosilicate glasses are made at relatively high-temperature[24 28 29] and iodine volatilizes at such high temperature, borosilicate glasses cannot dissolve large amount of iodine when adopting this protocol. Riley et al.[16] reported an iodine solubility up to 0.7 mol.% in Low Activity Waste (LAW) glass composition made at near ambient pressure (i.e. sealed-capsule). To bypass this low iodine dissolution level in borosilicate glass matrix, recent works[30 31 32 33] employed high-pressure conditions to increase drastically the iodine solubility in borosilicate glasses. For instance, recent work by Morizet et al.[33] measured iodine solubility up to ~6 mol.% in low-silica, high-boron, Ca- and Na-bearing glasses synthesized at 1.5 GPa. Jolivet et al.[32] measured up to 2.5 mol.% in LAW glasses synthesized at 1.5 GPa; representing four times the iodine solubility

measured at ambient pressure for comparable glass compositions[16 17 34]. This recent advance constitutes a potential solution for the future immobilization of ^{129}I; however, it requires assessing the durability of these I-bearing glasses synthesized under high-pressure conditions. To do so, a microscopic level of information is required to scrutinize the iodine speciation and its local environment at atomic scale when dissolved in the glass structure.

Recent studies demonstrated that such information can be accessed via X-ray Absorption Spectroscopy (XAS) and X-ray Photoelectron Spectroscopy (XPS)[16 17 30 33 34 35 36]. In particular, XPS measurements clearly identify when iodine is dissolved as iodide (I^-) or iodate (I^{5+}) in borosilicate glasses[33 36 37]. On the other hand, XAS studies have provided valuable information on the iodine atomic local environment as dissolved under its iodide form in borosilicate glasses[17 35 36]. Furthermore, XAS has been applied to characterize the iodine local environment in a wide variety of samples: from inorganic crystalline compounds[18 38 39 40 41 42 43] to organic[44 45]. For glasses, it was demonstrated that I^- anions dissolved in glasses were charge compensated by the available network modifying cations such as Na^+ or Ca^{2+}. The derived coordination number obtained from XAS spectrum modelling suggests that around four Na^+ contribute to charge balance I^-, while around two Ca^{2+} contribute to charge balance I^- in glasses, regardless of their synthesis conditions: ambient or high-pressure[17 36]. Concomitantly, to address the glass chemical durability, the effect of iodine dissolution on the glass structure has been recently discussed and suggests that iodine dissolution as I^- and forming Na-I clusters is likely to induce an increase in the degree of polymerization [34 36]. However, this is not clearly demonstrated and more advanced investigations (i.e. ^{17}O NMR) are required. For instance, Jolivet et al.[32] showed that the relative proportion of BO_4 (N_4 = $[BO_4] / [BO_4 + BO_3]$) could increase or decrease depending on the glass bulk composition.

All the recent works focused on the atomic local environment of iodide (I^-) surrounded by either Na^+ or Ca^{2+} to form Na-I and Ca-I clusters, respectively. Interestingly, it has been

inferred that iodide species correspond to one of the most stable inorganic form found in the environment; however, iodate could also be found noticeably[46 47]. So far, there has been no investigation on the atomic local environment for iodate species dissolved in glasses. Serendipitously, Morizet et al.[33] showed that the level of iodine solubility achieved in case of the iodate form is four times higher than in case of iodide; therefore representing a serious option for the immobilization of ^{129}I. Most iodine waste solid sorbents could be concerned by this approach (see Riley et al.[14] and reference therein). They also showed that increasing the oxidizing conditions could also promote the formation of periodate species (I^{7+}); although it was suggested that this fully oxidized species was not stable under X-ray excitation. Hence, the local atomic environment for iodate (and periodate) needs investigations in order to evaluate and compare the chemical durability of those I-bearing glass matrices in the case iodide (I^-) and iodate (I^{5+}) for future immobilization of ^{129}I-bearing nuclear wastes in natural repository geological site.

In the present work, we used I K-edge XAS to characterize and to compare at the atomic scale the local environment of iodine atoms dissolved in glasses in presence of iodide, iodate and periodate species. We studied the I-bearing glasses studied by Morizet et al.[33] and synthesized under high-pressure conditions (at identical pressure conditions) and for which I speciation has been fully determined using XPS measurements. For the first time, the atomic distances and coordination number to first and second next nearest neighbors have been determined for iodate species dissolved in aluminoborosilicate glasses. A discussion on the I-bearing glass chemical durability based on the I speciation and atomic environment is also proposed.

II. EXPERIMENTAL

A. Sample dataset

As described in Morizet et al.[33] the samples consist in clear brownish glasses synthesized under high-pressure conditions (1.5 GPa) and high-temperature (1400°C) and using different source of iodine (i.e. I_2 and I_2O_5) leading to different iodine dissolution mechanisms. The investigated glass compositions are aluminoborosilicate glasses prepared in the B_2O_3-SiO_2-Al_2O_3-CaO-Na_2O system. The description for glass synthesis is reported in the subsequent work[33]; however, we provide in Suppl. Mat. the reported glass compositions studied here: ~32 mol.% SiO_2, ~30 mol.% B_2O_3, 5 mol.% Al_2O_3 and ~35 mol.% CaO + Na_2O. In the investigated glasses, CaO and Na_2O are exchanged on a mole-to-mole basis, keeping the oxygen concentration constant. For instance, $C_{35}N_0$ stands for a glass without Na and C_0N_{35} stands for a glass without Ca. The investigated samples were fully characterized and especially the iodine solubility and speciation. X-ray Photoelectron Spectroscopy (XPS) revealed that 1) iodine is mostly dissolved under its iodide form (I^-) in the CN-1 glass series, 2) iodine is mostly dissolved under its iodate form (I^{5+}) in the CN-2 and CN-3 glass series and 3) iodine is also present under its periodate form (I^{7+}) in CN-3 glass series, however, this latter species appeared not to be stable under the X-ray beam during XPS analyses. Most of the samples reported in Morizet et al.[33] (see Table 1) were analyzed using XAS in conjunction with previously published XPS results to determine the local atomic environment (distance and coordination number to next nearest neighbor that is not reachable with XPS investigation) of the different iodine species dissolved in glasses.

In addition, crystalline compounds were also studied in order to conduct the fingerprinting for the interpretation of the XAS spectra for I-bearing glasses. Iodides (NaI and CaI_2), iodate ($NaIO_3$, CaI_2O_6), periodate ($NaIO_4$), I_2 and I_2O_5. Unfortunately, calcium periodate (CaI_2O_8) could not be acquired. Iodides are highly hygroscopic; hence, it is suspected that iodide have altered to an hydrated form as also pointed out in previous works[17].

B. X-ray Absorption Spectroscopy at the Iodine K-edge

X-ray Absorption Spectroscopy was conducted on the glass and crystalline samples at the I K-edge on SAMBA beamline at SOLEIL synchrotron facility operating with a current of 500 mA and 2.75 GeV[48]. We acquired the XAS spectra in both the X-ray Absorption Near-Edge Spectroscopy (XANES) and Extended X-Ray Absorption Fine Structure (EXAFS) regions. XAS acquisitions at the I K-edge (~33169 eV) were preferred instead of the I L_3-edge (~4557 eV) as in Morizet et al.[36] owing to the possible interferences provoked by the Ca K-edge line at ~4038 eV. The energy calibration was performed using a Sb reference foil with a first derivative absorption edge at 30491 eV. Spectrum acquisition was performed in transmission mode. Acquisitions were made in continuous scan mode from 200 eV below the iodine absorption edge (~33175 eV) up to 820 eV above the iodine absorption with a 0.5 eV energy step. The counting time on each point is 0.1 s. To obtain a suitable signal to noise ratio (S/N), at least 5 scans were acquired, however, at the lowest iodine content (CN-1 glass series) we had to collect more than 10 scans. Even using a cautious protocol, the obtained EXAFS signal for CN-1 samples remains weak in comparison to the EXAFS signal obtained for the glasses with the highest iodine content (CN-2 and CN-3 glass series). For crystalline compounds, only 3 scans were necessary for obtaining a suitable S/N. One scan recording time sums up to 204 s.

The glass powder was crushed, mixed with graphite powder, and pressed as a 6 mm in diameter pellet. We did not weight the mass of glass embedded in the pellet. The beam size is estimated to be 0.49 x 2.76 mm^2 that focuses on the sample pellet using two cylindrical mirror with a tilt angle of 1 mrad. The different ionization chambers were filled with Ar at 1000 mbar absolute pressure. Considering that some iodine species lack stability under an X-ray beam (i.e. I^{7+}), each spectrum was recorded at 20 K under liquid helium cryostatic conditions.

C. X-ray Absorption Spectroscopy spectral treatment

The normalization and data treatment were performed using Athena software package[49]. EXAFS signals were simulated using Artemis software package[49]. We employed the fingerprinting method for discussing the change in the XANES spectra in between the glass series. The EXAFS spectra were fitted using the scattering equation and standard crystalline structure obtained from the Crystallography Open Database (COD, see Vaitkus et al.[50] and references therein). Prior to the simulation of the EXAFS spectra for I-bearing glasses we determined the scattering amplitude (S_0^2) and the correction for the edge position (ΔE_0)[36 51]. We used the spectra obtained on crystalline $NaIO_3$ and the corresponding $NaIO_3$ structure from the COD and with a space group *Pbnm*. We derived an $S_0^2 = 0.909$ and $\Delta E_0 = 6.90$ eV.

The glass EXAFS spectra were fitted using several single scattering paths in agreement with the observation made from XPS results. For instance, in the CN-2 and CN-3 glass series, the first neighbor to iodine atoms are mostly oxygen in agreement with the iodate local environment determined by XPS. Hence, we used the single scattering path between I and O from either $NaIO_3$ or CaI_2O_6 structures. However, iodide species have also been identified and in that case the first nearest neighbor to iodine atoms (as I^-) is either Ca^{2+} or Na^+ forming Ca-I and Na-I local environment, respectively. For iodide the distance to first neighbor is on the order of 3 Å as shown in previous works[17 36]. This distance is comparable to the distance to second nearest neighbor for iodate structure ($r_{Na\text{-}I} = 3.52$ Å in $NaIO_3$). Hence, a single scattering for Na and Ca is added for simulating either the first nearest neighbor in the case of iodide or the second nearest neighbor in the case of iodate local environments for CN-2 and CN-3 glass series. Periodate species were identified in the case of $C_{35}N_0$-33 implying that the first nearest neighbor to iodine atoms is oxygen and the second nearest neighbor is calcium and the single scattering paths were chosen accordingly. The simulation of the CN-1 glass series EXAFS spectra was more complicated owing to the short EXAFS signal in k-space in

addition to the lower I content measured in these glasses. However, previous investigations showed that in the case of iodide, the first nearest neighbor in local environment to iodine atoms is either Ca^{2+} or Na^{+}[17 36]. As a result, we used I to Na and I to Ca paths for the simulation of iodide local environments in CN-1 glasses. We show that the sole use of those paths is not sufficient for fully reproducing the EXAFS spectra and single scattering path I to O is required. It is in favor of the possible presence of iodate species (not identified by XPS) that could result from sample oxidation through time. Furthermore, the scattering path from I to I for I_2 species was required for a reliable simulation of the EXAFS signal for $C_{35}N_0$-1. The use of single scattering path from I to I for I_2 species is justified by the identified presence of I^0 species by XPS measurements (see Table 1). However, we did not use systematically the scattering path for I_2 species, even though it was identified via XPS measurements in Morizet et al.[33], as the addition of the I_2 single scattering path to the simulation did not significantly improve the result of the fit.

Simulations were conducted with the following protocol to obtain 1) the coordination number (CN_{I-X}), 2) the distance to the atom counterpart (r_{I-X}) and 3) the Debye-Waller factor (σ_{I-X}). The coordination number initialization was set as follow: the CN_{I-O}, CN_{I-Na}, CN_{I-Ca} and CN_{I-I} are 3, 4, 2 and 1, respectively. The coordination number for Na and Ca is consistent with the results reported in previous XAS investigations[17 36]. We applied a CN_{I-O} = 3 in agreement with the local environment for iodate species, nonetheless we apply the same CN_{I-O} for $C_{35}N_0$-33 in which periodate species have been identified and would therefore require a CN_{I-O} = 4. In detail, we will show and discuss the fact that the distinction between IO_3^- and IO_4^- is impossible using the EXAFS signal. The Debye-Waller factor was initially set to 0.003 for each path. The distance to first neighbor was set at the standard distance of each crystallographic structure: r_{I-O} = 1.79 Å from $NaIO_3$, r_{I-Na} = 3.27 Å from NaI, r_{I-Ca} = 3.12 Å from CaI_2 and r_{I-I} = 3.54 Å from I_2. The first parameter to be optimized is the distance

between iodine atoms and the nearest neighbor (r_{I-X}) for the whole set of scattering paths, then followed by the optimization of the coordination number between iodine atoms and the nearest neighbor (CN_{I-X}) for the whole set of scattering paths. These optimizations are repeated three times, and then the Debye-Waller factors (σ_{I-X}) are optimized. In the final round, the three parameters are successively optimized. In the case that the optimization is not entirely successful, the optimization of the three sets of parameters is conducted again to reach an acceptable fit (i.e. based on r^2 value). We should point out that the proposed simulations are one possible solution amongst others.

III. RESULTS AND DISCUSSION

A. I K-edge XANES

We show the XANES spectra obtained at the I K-edge for crystalline compounds in Figure 1. The spectra are shown in increasing order of oxidation state from reduced (-1 for NaI and CaI_2) to intermediate oxidation state (0 for I_2, +5 for I_2O_5, $NaIO_3$ and CaI_2O_6) to high oxidation state (+7 for $NaIO_4$). We observe that reduced crystalline compounds (NaI, CaI_2 and I_2) are relatively featureless in comparison to oxidized crystalline standards (I_2O_5 and $NaIO_3$), which have an obvious post-edge structure. The XANES spectra observed for NaI, CaI_2 and I_2 are consistent with previous works[17 30 35 52]. Strangely, oxidized standards do not show the same spectrum line shape. For instance, $NaIO_3$ and I_2O_5 exhibit a strong peak located at 33178 eV whereas it is not visible for $NaIO_4$ and CaI_2O_6. This peak is also reported in previous studies for oxidized iodate compounds[17 35 39]. Although to our knowledge XANES spectra for $NaIO_4$ have never been published, we believe that $NaIO_4$ and CaI_2O_6 have probably quickly destabilized prior to the XAS acquisition. Using the edge first derivative did not show a systematic change as a function of the redox state of the crystalline standard.

Nonetheless, the distinction between reduced and oxidized iodine local environment can be made.

The XANES spectra obtained for the three series of glasses are shown in Figure 2: Figure 2A for CN-1, Figure 2B and C for CN-2 and 3, respectively. The iodine speciation expressed as the molar fraction of I^{5+} is also reported. When comparing XANES spectra with those of the reference compounds, samples of the CN-1 series contain predominantly I^- and samples of the CN-2 and CN-3 series contain mainly IO_3^-. The spectra for CN-2 and CN-3 glass series exhibit a strong feature at ~33178 eV that is also observed for crystalline $NaIO_3$ and I_2O_5 (see Figure 1). The featureless aspect of the CN-1 glass series spectra is consistent with the spectra recorded for NaI and CaI_2. We do not observe any difference in between the spectrum obtained for $C_{35}N_0$-2 and the spectrum obtained for $C_{35}N_0$-33. It is rather surprising considering that the $C_{35}N_0$-33 glass contains periodate species (I^{7+}) suspected to be surrounded by four oxygen atoms to form IO_4^- units. We expected a slight change in the spectrum line shape with the appearance of I^{7+} species. In between the glass compositions we do not observe any change in the main line, edge position or post-edge peak positions suggesting that the iodine local environment is similar for the glass compositions explored here. The position of the main line for CN-2 and CN-3 glass series ranges from 33178.3 to 33179.3 eV. The position of the edge ranges from 33173.6 to 33177.6 eV but does not exhibit systematic change as function of the glass XNa or I content. To a first level of knowledge, the I K-edge XANES spectra can be used to determine the iodine oxidation state in glasses, for instance using linear combination analyses with spectra of model compounds[36 53]; however, this approach appears relatively inaccurate in determining the iodine speciation dissolved in glasses using model spectra from crystalline compounds (see Morizet et al.[36]).

B. I K-edge EXAFS

The EXAFS amplitude of the pseudo Radial Distribution Function (RDF) for crystalline standards is shown in Figure 3. This amplitude was obtained from the Fourier transforms of the oscillatory k^2-weighted. Again, we categorize the spectra with increasing oxidation state from reduced compounds (NaI and CaI_2) to oxidized ones ($NaIO_3$, CaI_2O_6 and $NaIO_4$). The most intense peak on the RDF spectra represents the signature of the first neighbor to iodine. The indicated values correspond to the apparent peak maximum and not to the actual distance between I atom and its nearest neighbor owing to the mathematical form of the Fourier transform. The actual distance between I atom and its first neighbor is obtained by addition of ~0.5 Å. Nonetheless, we observe that the distance to the iodine first neighbor is shorter in the case of iodate and periodate than in iodide. This is consistent with the standard crystalline structure with $r_{I\text{-}O} \approx 1.8$ Å in iodates and periodates, with $r_{I\text{-}Na\ or\ Ca} \approx 3.2$ Å in iodides. We also observe a strong signal above 4 Å in NaI spectrum which could correspond to a potential hydration of the crystalline powder as inferred earlier and asserted in previous works[17].

The k-space data for investigated glasses are shown in Figure 4 and categorized as a function composition: Figure 4A for C_{35}, Figure 4C for C_{20} and Figure 4E for C_0 glass compositions. The oscillatory spectra represent the $k^2\chi(k)$ data treated by Fourier transform of the EXAFS signal up to ~800 eV above the edge position leading to a wavenumber extending up to 14 $Å^{-1}$ in the k-space. It should be emphasized that an identical treatment was applied to all spectra for adequate comparison.

The first striking observation in Figure 4 is that the S/N is far better for glasses from the CN-2 and CN-3 series than for the CN-1 series. Currently, we do not have a clear explanation for that and we only have hypotheses. In Figure 4A, the S/N of the spectra is changing for almost an identical I content suggesting that the total I in mol.% is not responsible for the lower S/N in the CN-1 glass series. Although, we did not weigh the sample mass powder introduced to the pellet, we suspect that the lower S/N is ascribed to a lower quantity of CN-1 glass

297 powders introduced in the pellet. Nevertheless, in order to be comparable we considered a
298 constant k range for all the samples from 3 to 12 $Å^{-1}$ to obtain the RDF spectra.

299 The second observation is that the k-space signal observed for CN-2 and CN-3 glasses
300 appears almost identical. For these glass series, the k space signal is also comparable in
301 between the glass compositions. These two features are anticipated owing to the comparable
302 identified iodine speciation measured in those glasses. On the contrary, the k space signal is
303 different (i.e. shifted phase in comparison to CN-2 and CN-3) for glasses obtained in the CN-
304 1 series. Again, this aspect is due to the change in iodine speciation. The glass corresponding
305 RDF is provided in Figure 4B, D and F for the same glass compositions and with the iodine
306 reported as the molar fraction of iodate species (XI^{5+}). The glasses with iodate identified as
307 the main iodine species (CN-2 and CN-3) exhibit a strong signal at short distance in the RDF
308 (~1.3 Å) whereas the glasses with iodide identified as the main iodine species (CN-1) seem to
309 have their first neighbor signal at longer distance at ~2.6 Å. For this later glass series, we also
310 observe the presence of additional peaks at lower distance (especially visible for C_0N_{35}-11)
311 which could be ascribed to the presence of iodine species with a local environment close to
312 the one observed for iodate environments. The presence of more oxidized iodine local
313 environments (i.e. iodate) in C_0N_{35}-11 glass have not been shown from the XPS
314 measurements in Morizet et al.[33]. One possible explanation for the presence of oxidized
315 species could be a possible slight alteration of the iodine speciation through time of C_0N_{35}-11
316 samples. Another hypothesis is that the XPS measurements from Morizet et al.[33] failed to
317 identify the presence of iodate species in C_0N_{35}-11 sample within the bulk of the glass.

318 The fitting of the EXAFS data is shown in Figure 5 for four different glass compositions:
319 $C_{35}N_0$, $C_{30}N_5$, $C_{20}N_{15}$ and C_0N_{35}. The RDF has been fitted following the protocol described in
320 the experimental section and the entire set of fit can be found in the Suppl. Mat. We show the
321 fit of the RDF of the magnitude along with the fit of the imaginary part of the RDF. The

derived distances (r_{I-X}), coordination number (CN_{I-X}) and Debye-Waller factor (σ_{I-X}) are also reported and the whole set of derived parameters are given in Table 1. The reported error bars on the distances and coordination numbers are obtained from Artemis software package[49]. As can be seen in Figure 5 the RDF region fitted is dependent on the glass series. For instance, the CN-2 and CN-3 glasses were fitted between 1 and 3 Å; whereas the fitted RDF region is extending up to 3.5 Å for the CN-1 glasses. Clearly, it can be seen that the fit quality obtained for the CN-2 and CN-3 glasses is far better than for the CN-1 glass. This is explained by the fact that the EXAFS signal quality in k-space shown in Figure 4 has an excellent S/N in CN-2 and CN-3 in comparison to CN-1.

The derived data (r_{I-X} and CN_{I-X} from Table 1) are plotted in Figure 6 as a function of iodine content in mol.%. For clarity, the error on the I content is not reported, however, it has been quantified at ±0.1 mol.%[33]. The change in the r_{I-X} distances is shown in Figure 6A for the whole glass series. Regardless of the glass composition and glass series, the distance between iodine atoms and first nearest oxygen in the iodate configuration is on average constant at r_{I-O} = 1.79±0.01 Å which compares adequately to the r_{I-O} distance observed in crystalline iodates ($r_{I-O} \approx 1.8$ Å). The distinction between iodate and periodate species is not possible on the sole criterion of the first neighbor distance. The distance to either the second nearest neighbor for iodate and periodate or the first nearest neighbor for iodide is also roughly constant for Na and Ca with r_{Na-I} and r_{Ca-I} at ~3.18±0.06 and ~3.20±0.12, respectively. These distances also compare adequately with the equivalent distance in crystalline compounds at ~3.2 Å. Like for the r_{I-O}, from the derived data plotted in Figure 6A we cannot make the distinction between the first and second nearest neighbor configuration in iodate (or periodate) and iodide.

Whereas the change in the first neighbor distance can be plotted for the whole set of glass series, we could not plot the change in the coordination number for the CN-1 glasses due to the important scatter in the derived coordination number (see Table 1). For example, the CN_{I-}

$_{Na}$ ranges from 2.2±0.4 to 4.1±1.3 and $CN_{I\text{-}Ca}$ ranges from 0.8±0.3 to 1.9±0.2. Although there is a large dispersion in the derived $CN_{I\text{-}Na\ or\ Ca}$ values, we observe that the $CN_{I\text{-}Na}$ is systematically higher than the $CN_{I\text{-}Ca}$, probably because of the lower positive charges on sodium. Comparable results have been found in Morizet et al.[36] for glasses of different compositions demonstrating that I^- requires more charge compensating cations in its surrounding in the case of Na^+ rather than Ca^{2+}. Invariably, the iodine coordination to oxygen in iodate configuration is close to 3 with $CN_{I\text{-}O}$ = 3.0±0.2 in adequate comparison to the structure of crystalline iodate. However, the distinction between iodate and periodate configuration seems unachievable using EXAFS and the distinction must be combined to another analytical technique such as the XPS method. Surprisingly, we derived a lower coordination between I and the second coordination sphere with Ca and Na in the case of $C_{35}N_0$-2 and C_0N_{35}-2. For instance the $CN_{Na\text{-}I}$ strongly drops from 2.8 to 0.8 between $C_{20}N_{15}$-2 and C_0N_{35}-2 (see Table 1). The $CN_{Ca\text{-}I}$ decrease is less pronounced between $C_{30}N_5$-2 and $C_{35}N_0$-2: from 1.9 to 1.2. One possible explanation to this peculiar result is that in the case of both, the Ca and the Na free glass samples, there is no mixed alkali effect[54] that could induce an aggregation of Na^+ cations forming a Na-rich area. Instead Na^+ are fully dispersed throughout the glass structure. As a result, the solution mechanism for IO_3^- and the average repartition of Na^+ cations does not allow the clustering of several Na^+ surrounding IO_3^-.

Whereas XPS is able to investigate the actual iodine speciation from the qualitative and quantitative point of view based on a surface analyses (only a few nm depth), the EXAFS is able to probe in depth the atomic structure and the iodine local environment at the Å scale. Both types of information are required for improving our current knowledge on the iodine dissolution mechanisms into the borosilicate glass matrix with the purpose of building a specific matrix for the immobilization of ^{129}I radioisotopes.

C. Structural model for iodine solution in glasses: Insight into the I-bearing glass durability

Recently, strong efforts have been made to constrain the iodine solution mechanism in borosilicate glass matrices[14 17 16 30 31 32 33 34 35 36]. The main objective is to propose a formulation of a specific glass composition in which iodine can be dissolved in large quantity and that is stable. The question of the I-bearing glass chemical durability is currently weakly addressed and only recent work[55] has focused on the release of iodine from a borosilicate glass matrix through leaching experiments by aqueous solution. This information is essential considering the issue on the ^{129}I radioisotopes in the environment and for safety assessment[46].

On the basis of the results obtained from EXAFS simulations, we have constructed a schematic view of the local environment of iodine atoms in the case of pure sodic glass composition (C_0N_{35}) in Figure 7: in iodide configuration (Figure 7A) and iodate configuration (Figure 7B). The common feature in between the two molecular configuration is the distance to the positive charge compensator that is on the order of 3.2 Å (i.e. it applies to all glass compositions whether it is Na^+ or Ca^{2+}). As described earlier, the local environment of iodine for iodate species is the surrounding of 3 oxygen atoms at a distance of 1.8 Å. The same applies to the mixed Ca-Na or pure Ca glass compositions. As discussed above, C_0N_{35}-2 represents a particular case as a single Na^+ is requested for the charge compensation of the IO_3^- cluster; which we attribute to the absence of mixed alkali effect.

Addressing the glass durability is not trivial considering the many involved mechanisms: diffusion rate, ion exchange, structural bond strength and hydration free energy[56]. As recently mentioned by Abdelouas et al.[57], it is difficult to predict the corrosion for glasses with multicomponent composition, as is our case. Moreover, if recent work by Zhang et al.[55] quantified the release of iodine dissolved as iodide (I^-) in strongly polymerized borosilicate glasses (i.e. International Simple Glass[24]), the question of the iodine release remains open in

the case of iodine dissolved as iodate (IO_3^-) and for depolymerized borosilicate glass compositions such as the CN glass series. Consequently, specific experiments must be conducted to answer these points.

The glass chemical durability is strongly influenced by the concentration of network modifying cation: the glass durability decreases with increasing concentration of network modifying cation[57]. However, the nature of the network modifying cation itself has an impact on the glass durability. For instance, the Na_2O-bearing glass durability is increased in the case Na_2O is accompanied by divalent cations such as CaO[57]. In the present study, regardless of the alteration conditions (i.e. inherent to environmental conditions), it implies that compositions such as $C_{10}N_{25}$ or $C_{20}N_{15}$ are likely to have a better resistance to alteration than C_0N_{35}. This is probably ascribed to the mixed alkali or alkaline-earth effect in which Na^+ and Ca^{2+} are mixing together to obtain a more stable glass configuration and both cations are charge compensating the negative charges carried by the Non-Bridging Oxygens (NBOs) of the glass network[54 58].

The present investigated CN glass composition are strongly enriched with respect to alkali or alkaline-earth (~35 mol.%) and are rather silica-poor (<35 mol.%). Hence, these glass compositions are likely to alter quickly upon leaching experiments and therefore do not represent fully adequate candidates for the ^{129}I immobilization in a durable manner. More suitable glass formulation is required, for instance with less network modifying cation and less B_2O_3. However, the possible glass corrosion by H^+ forming SiOH molecular groups is questionable. The CN glass composition is depolymerized in nature owing to the high network modifying cation concentration. It implies a high NBOs concentration. As a result, the mechanism to form SiOH groups and involving Si-O-Si bond is probably reduced owing to the strong depolymerization nature of the glass composition.

Nevertheless, because iodine dissolution is likely to induce a slight polymerization as suggested in previous works[33 34 36]; therefore Si-O-Si bonds are formed because of the Na^+ consumed for iodine species charge compensation. In that case, the hydrolysis of Si-O-Si by H^+ to form SiOH groups is therefore possible. So far, there is only one study that addressed the iodine release from I-bearing aluminoborosilicate glasses from Zhang et al.[55]. Further work is currently required to address the iodine release from aluminoborosilicate glasses under various configurations and with different glass compositions: from iodide to iodate, with various network modifying cations and in glasses with different degrees of polymerization. In addition, alteration under different regime: solution temperature and solution pH, has to be conducted for investigating the stability of iodine species[7].

IV. CONCLUSIONS

In the present work, we have investigated the local atomic environment around iodine dissolved in glasses using XAS. For a series of aluminoborosilicate glasses synthesized under pressure and having different iodine content (up to 6 mol.%) and different iodine speciation (ranging from I^- to I^{7+}) we have determined the distance between iodine atom and its first nearest neighbor and its coordination number.

In particular, we provide the first structural data for iodine dissolved in glasses as iodate. Iodate clusters show the expected local structure with 3 neighboring oxygen atoms and at a distance of ~1.8 Å surrounding the I^{5+} cation forming IO_3^-. At longer distance Na^+ and Ca^{2+} are the charge compensating the negative charge of the IO_3^- unit with an average of ~3 Na^+ and 1.5 Ca^{2+} cation surrounding the IO_3^- cluster.

SUPPLEMENTARY MATERIAL

See Supplementary Material for the investigated glass compositions and the fit to I K-edge EXAFS data.

ACKNOWLEDGEMENTS

The authors are grateful to the Agence Nationale de la Recherche and Région Pays de la Loire, which financed the current work through the ANR project "Iodine-CLEAN-UP" (ANR-20-CE08-0018) and the Pari Scientifique "CIPress". The authors thank the Laboratoire de Planétologie et Géosciences, the Institut des Matériaux Jean Rouxel, the University of Nantes and the CNRS for providing access to the analytical facilities. We acknowledge SOLEIL for provision of synchrotron radiation facilities and we would like to thank SAMBA staff for assistance in using the beamline.

REFERENCES

[1] C.W. Abney, Y. Nan, and L.L. Tavlarides, Ind. Eng. Chem. Res. **56**, 4837 (2017).
[2] A.-L. Chabauty, L. Campayo, F.O. Méar, and L. Montagne, Journal of Non-Crystalline Solids **510**, 51 (2019).
[3] IAEA and International Atomic Energy Agency, *Climate Change and Nuclear Power 2020* (2020).
[4] B.W. Brook, A. Alonso, D.A. Meneley, J. Misak, T. Blees, and J.B. van Erp, Sustainable Materials and Technologies **1–2**, 8 (2014).
[5] D. Caurant and O. Majérus, in *Encyclopedia of Materials: Technical Ceramics and Glasses* (Elsevier, 2021), pp. 762–789.
[6] A. Aldahan, V. Alfimov, and G. Possnert, Applied Geochemistry **22**, 606 (2007).
[7] X. Hou, V. Hansen, A. Aldahan, G. Possnert, O.C. Lind, and G. Lujaniene, Analytica Chimica Acta **632**, 181 (2009).
[8] X. Chen, M. Gong, P. Yi, A. Aldahan, Z. Yu, G. Possnert, and L. Chen, Nuclear Instruments and Methods in Physics Research Section B: Beam Interactions with Materials and Atoms **361**, 604 (2015).
[9] R. Michel, A. Daraoui, M. Gorny, D. Jakob, R. Sachse, L. Tosch, H. Nies, I. Goroncy, J. Herrmann, H.-A. Synal, M. Stocker, and V. Alfimov, Science of The Total Environment **419**, 151 (2012).
[10] E. Englund, A. Aldahan, X.L. Hou, G. Possnert, and C. Söderström, Nuclear Instruments and Methods in Physics Research Section B: Beam Interactions with Materials and Atoms **268**, 1139 (2010).
[11] Y. Fan, X. Hou, W. Zhou, and G. Liu, Journal of Environmental Radioactivity **154**, 15 (2016).
[12] P. He, X. Hou, A. Aldahan, and G. Possnert, J Radioanal Nucl Chem **299**, 249 (2014).
[13] Q. Hu, P. Zhao, J.E. Moran, and J.C. Seaman, Journal of Contaminant Hydrology **78**, 185 (2005).

[14] B.J. Riley, J.D. Vienna, D.M. Strachan, J.S. McCloy, and J.L. Jerden, Journal of Nuclear Materials **470**, 307 (2016).
[15] T. Lemesle, F.O. Méar, L. Campayo, O. Pinet, B. Revel, and L. Montagne, Journal of Hazardous Materials **264**, 117 (2014).
[16] B.J. Riley, M.J. Schweiger, D.-S. Kim, W.W. Lukens, B.D. Williams, C. Iovin, C.P. Rodriguez, N.R. Overman, M.E. Bowden, D.R. Dixon, J.V. Crum, J.S. McCloy, and A.A. Kruger, Journal of Nuclear Materials **452**, 178 (2014).
[17] D.A. McKeown, I.S. Muller, and I.L. Pegg, Journal of Nuclear Materials **456**, 182 (2015).
[18] L. Campayo, A. Grandjean, A. Coulon, R. Delorme, D. Vantelon, and D. Laurencin, J. Mater. Chem. **21**, 17609 (2011).
[19] L. Campayo, S. Le Gallet, D. Perret, E. Courtois, C. Cau Dit Coumes, Yu. Grin, and F. Bernard, Journal of Nuclear Materials **457**, 63 (2015).
[20] A. Coulon, A. Grandjean, D. Laurencin, P. Jollivet, S. Rossignol, and L. Campayo, Journal of Nuclear Materials **484**, 324 (2017).
[21] S. Chong, J.A. Peterson, B.J. Riley, D. Tabada, D. Wall, C.L. Corkhill, and J.S. McCloy, Journal of Nuclear Materials **504**, 109 (2018).
[22] S. Chong, B.J. Riley, R.M. Asmussen, A.R. Lawter, S.H. Bruffey, J. Nam, J.S. McCloy, and J.V. Crum, Journal of Nuclear Materials **538**, 152222 (2020).
[23] J.O. Kroll, B.J. Riley, J.S. McCloy, and J.A. Peterson, J Sol-Gel Sci Technol **96**, 564 (2020).
[24] S. Gin, A. Abdelouas, L.J. Criscenti, W.L. Ebert, K. Ferrand, T. Geisler, M.T. Harrison, Y. Inagaki, S. Mitsui, K.T. Mueller, J.C. Marra, C.G. Pantano, E.M. Pierce, J.V. Ryan, J.M. Schofield, C.I. Steefel, and J.D. Vienna, Materials Today **16**, 243 (2013).
[25] F. Angeli, T. Charpentier, D. De Ligny, and C. Cailleteau, Journal of the American Ceramic Society **93**, 2693 (2010).
[26] J. de Bonfils, S. Peuget, G. Panczer, D. de Ligny, S. Henry, P.-Y. Noël, A. Chenet, and B. Champagnon, Journal of Non-Crystalline Solids **356**, 388 (2010).
[27] D. Holland, B.G. Parkinson, M.M. Islam, A. Duddridge, J.M. Roderick, A.P. Howes, and C.R. Scales, Appl Magn Reson **32**, 483 (2007).
[28] B.K. Maji, H. Jena, and R. Asuvathraman, Journal of Non-Crystalline Solids **434**, 102 (2016).
[29] M.J. Plodinec, Glass Technol. **41**, 186 (2000).
[30] M.R. Cicconi, E. Pili, L. Grousset, P. Florian, J.C. Bouillard, D. Vantelon, and D.R. Neuville, Sci Rep **9**, 7758 (2019).
[31] M.R. Cicconi, E. Pili, L. Grousset, and D.R. Neuville, MRS Advances **4**, 971 (2019).
[32] V. Jolivet, Y. Morizet, M. Paris, and T. Suzuki-Muresan, Journal of Nuclear Materials **533**, 152112 (2020).
[33] Y. Morizet, J. Hamon, C. La, V. Jolivet, T. Suzuki-Muresan, and M. Paris, J. Mater. Chem. A **9**, 23902 (2021).
[34] B. Vénague, L. Campayo, M.J. Toplis, T. Charpentier, M. Moskura, and J.-L. Dussossoy, Journal of Non-Crystalline Solids **576**, 121278 (2022).
[35] I.S. Muller, D.A. McKeown, and I.L. Pegg, Procedia Materials Science **7**, 53 (2014).
[36] Y. Morizet, V. Jolivet, N. Trcera, T. Suzuki-Muresan, and J. Hamon, Journal of Nuclear Materials **553**, 153050 (2021).
[37] V. Jolivet, Y. Morizet, J. Hamon, M. Paris, and T. Suzuki-Muresan, J. Am. Ceram. Soc. **104**, 1360 (2021).
[38] D. Laurencin, D. Vantelon, V. Briois, C. Gervais, A. Coulon, A. Grandjean, and L. Campayo, RSC Adv. **4**, 14700 (2014).
[39] J. Podder, J. Lin, W. Sun, S.M. Botis, J. Tse, N. Chen, Y. Hu, D. Li, J. Seaman, and Y. Pan, Geochimica et Cosmochimica Acta **198**, 218 (2017).
[40] Y.S. Shimamoto and Y. Takahashi, Anal. Sci. **24**, 405 (2008).
[41] S. Kodama, Y. Takahashi, K. Okumura, and T. Uruga, Science of The Total Environment **363**, 275 (2006).
[42] M. Fuhrmann and S. Bajt, 15 (n.d.).

[43] I. Bonhoure, A.M. Scheidegger, E. Wieland, and R. Dähn, Radiochimica Acta **90**, 647 (2002).
[44] M.C. Feiters, F.C. Küpper, and W. Meyer-Klaucke, J Synchrotron Rad **12**, 85 (2005).
[45] Y.S. Shimamoto, Y. Takahashi, and Y. Terada, Environ. Sci. Technol. **45**, 2086 (2011).
[46] R.C. Moore, C.I. Pearce, J.W. Morad, S. Chatterjee, T.G. Levitskaia, R.M. Asmussen, A.R. Lawter, J.J. Neeway, N.P. Qafoku, M.J. Rigali, S.A. Saslow, J.E. Szecsody, P.K. Thallapally, G. Wang, and V.L. Freedman, Science of The Total Environment **716**, 132820 (2020).
[47] D.S. Hardisty, T.J. Horner, S.D. Wankel, J. Blusztajn, and S.G. Nielsen, Chemical Geology **532**, 119360 (2020).
[48] V. Briois, E. Fonda, S. Belin, L. Barthe, C. La Fontaine, F. Langlois, M. Ribbens, and F. Villain, in *UVX 2010 - 10e Colloque Sur Les Sources Cohérentes et Incohérentes UV, VUV et X ; Applications et Développements Récents* (EDP Sciences, Ile de Porquerolles, France, 2011), pp. 41–47.
[49] B. Ravel and M. Newville, J Synchrotron Rad **12**, 537 (2005).
[50] A. Vaitkus, A. Merkys, and S. Gražulis, J Appl Crystallogr **54**, 661 (2021).
[51] Y. Morizet, N. Trcera, C. Larre, M. Rivoal, E. Le Menn, D. Vantelon, and F. Gaillard, Chemical Geology **510**, 91 (2019).
[52] W.A. Reed, I. May, F.R. Livens, J.M. Charnock, A.P. Jeapes, M. Gresley, R.M. Mitchell, and P. Knight, J. Anal. At. Spectrom. **17**, 541 (2002).
[53] M.L. Schlegel, P. Reiller, F. Mercier-Bion, N. Barré, and V. Moulin, Geochimica et Cosmochimica Acta **70**, 5536 (2006).
[54] S.K. Lee and J.F. Stebbins, J. Phys. Chem. B **107**, 3141 (2003).
[55] H. Zhang, T. Suzuki-Muresan, Y. Morizet, S. Gin, and A. Abdelouas, Npj Mater Degrad **5**, 10 (2021).
[56] D.M. Strachan and T.L. Croak, 12 (2000).
[57] J.D. Musgraves, J. Hu, and L. Calvez, editors , *Springer Handbook of Glass* (Springer International Publishing, Cham, 2019).
[58] K.E. Kelsey, J.R. Allwardt, and J.F. Stebbins, Journal of Non-Crystalline Solids **354**, 4644 (2008).

FIGURE CAPTION

Figure 1: I K-edge XANES spectra obtained for crystalline standard compounds. The spectra are stacked from the most reduced (i.e. iodide with I^- oxidation state) to the more oxidized (periodate with I^{7+} oxidation state).

Figure 2: I K-edge XANES spectra obtained for the I-bearing CN glasses studied in Morizet et al.[33] The spectra are categorized on the basis of the iodine speciation from XPS measurements: CN-1 with iodide (I^-) as the main species, Figure 2A; CN-2 with iodate (I^{5+}) as the main species, Figure 2B; and CN-3 with iodate as the main species but also showing the presence of periodate (I^{7+}) in $C_{35}N_0$-33, Figure 2C.

Figure 3: Radial Distribution Function (RDF) obtained from k-space signal of the EXAFS spectra for crystalline compounds. The spectra are shown from the most reduced (i.e. iodide

with I^- oxidation state) to the more oxidized (periodate with I^{7+} oxidation state). An indication of the distance between iodine atoms and the first nearest neighbor is represented by the most intense peak in the RDF spectrum.

Figure 4: k^2-space signal obtained from the EXAFS spectra and the corresponding RDF spectrum for glasses of different compositions: $C_{35}N_0$ (A and B), $C_{20}N_{15}$ (C and D), and C_0N_{35} (E and F).

Figure 5: Results of the EXAFS fit for several glasses of different compositions and from different series. The absolute amplitude fit ($|\chi(R)|$ in $Å^{-3}$) is shown along with the fit of the imaginary part ($|\chi(R)$ Img| in $Å^{-3}$). The fitted region is also shown. The derived coordination numbers (CN_{I-X}) and nearest neighbor distance (r_{I-X}) is also reported and also provided in Table 1.

Figure 6: Change in the iodine to nearest neighbor (r_{I-X}, Figure 6A) and iodine coordination number (CN_{I-X}, Figure 6B) as a function of iodine content. Data are shown as a function of the glass category: CN-1, CN-2 and CN-3. Due to the large scatter obtained from the fit, the coordination numbers obtained on CN-1 glass series is not shown. The reported error bars (see Table 1) are the ones obtained from the fitting procedure using Artemis EXAFS fitting package[49]. For clarity, the error on the iodine content is not reported and is on the order ±0.1 mol.% as provided in Morizet et al.[33]

Figure 7: Schematic representation of the local environment for iodine dissolution. We propose a representation for Na-rich glass composition with iodide (I^-) and iodate (IO_3^-) local environments in Figure 7A and B, respectively.

Table 1: I K-edge EXAFS fitting results (coordination number CN, distance r and Debye-Waller factor σ) for I-bearing glasses with different I speciation: I^- (CN-1), I^{5+} (CN-2 and CN-3) and I^{7+} (CN-3).

Sample[a]	I content (mol.%)[a]	I speciation[a]				Oxygen			Sodium			Calcium			Iodine		
		I^-	I^0	I^{5+}	I^{7+}	r_{I-O}	CN_{I-O}	σ_{I-O}	r_{I-Na}	CN_{I-Na}	σ_{I-Na}	r_{I-Ca}	CN_{I-Ca}	σ_{I-Ca}	r_{I-I}	CN_{I-I}	σ_{I-I}
$C_{35}N_0$-1	1.2	93.9	6.1	0		1.73(1)[b]	3.5(12)	0.087(11)				3.26(4)	1.9(2)	0.016(2)	2.80(1)	0.3(1)	0.004(2)
$C_{20}N_{15}$-1	0.5	94.1	5.9	0		1.79(2)	0.3(1)	0.003(2)	3.28(1)	2.9(4)	0.002(2)	3.24(1)	1.7(2)	0.008(1)			
$C_{10}N_{25}$-1	1.7	85.2	14.8	0		1.79(1)	0.4(1)	0.003(3)	3.19(1)	2.2(4)	0.006(3)	3.1(2)	0.8(3)	0.006(4)			
C_0N_{35}-11	3.9	96.0	0	4.0		1.79(1)	0.6(1)	0.002(2)	3.25(2)	4.1(13)	0.021(7)						
$C_{35}N_0$-2	1.3	28.8	12.7	58.6		1.81(0)	2.9(2)	0.002(1)				3.38(6)	1.2(7)	0.005(9)			
$C_{30}N_5$-2	2.0	14.5	0	85.5		1.80(0)	3.1(1)	0.002(1)	3.16(4)	3.6(6)	0.006(5)	3.10(4)	1.9(4)	0.006(5)			
$C_{20}N_{15}$-2	4.8	9.2	8.2	82.5		1.80(0)	3.3(1)	0.002(1)	3.14(6)	2.8(7)	0.008(4)	3.07(7)	1.5(5)	0.008(4)			
C_0N_{35}-2	5.7	21.5	1.3	77.2		1.81(0)	2.7(1)	0.002(1)	3.19(6)	0.8(6)	0.003(9)						
$C_{35}N_0$-33	1.3	14.5	4.3	51.0	30.3	1.80(0)	3.1(2)	0.002(1)				3.37(6)	0.9(9)	0.005(9)			
$C_{20}N_{15}$-3	2.5	28.5	0	71.5		1.80(0)	2.8(1)	0.000(0)	3.08(3)	3.6(6)	0.007(6)	3.16(3)	1.7(8)	0.006(6)			
$C_{10}N_{25}$-3	5.0	21.8	0	78.2		1.80(0)	3.2(1)	0.002(1)	3.14(4)	3.7(7)	0.008(3)	3.06(4)	2.0(4)	0.008(3)			

[a] The investigated samples were obtained from Morizet et al.[33]. The I solubility data and I speciation obtained from XPS measurement are also reported.

[b] The figure between brackets corresponds to the standard error on the last digit reported after the fit by Artemis fitting package.

595

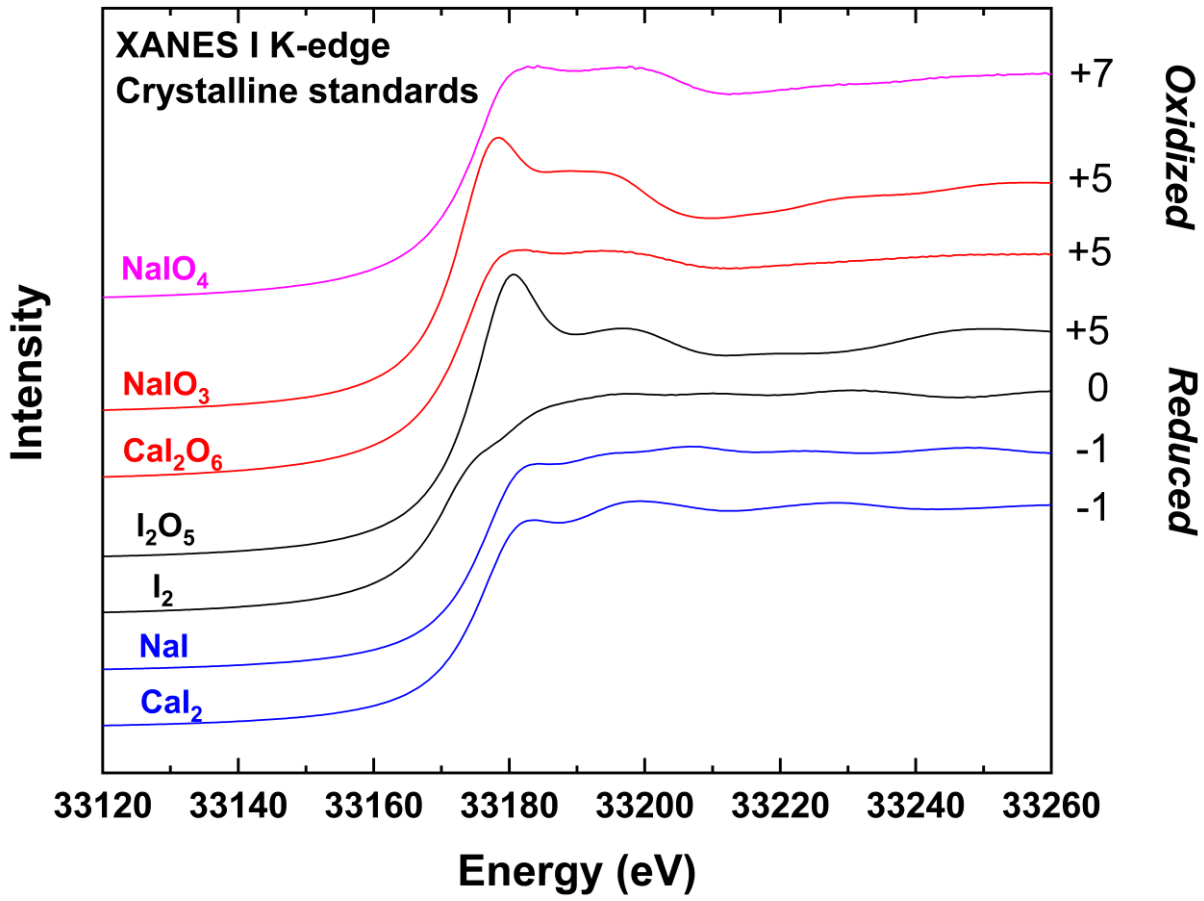

596

597 Figure 1

598

599

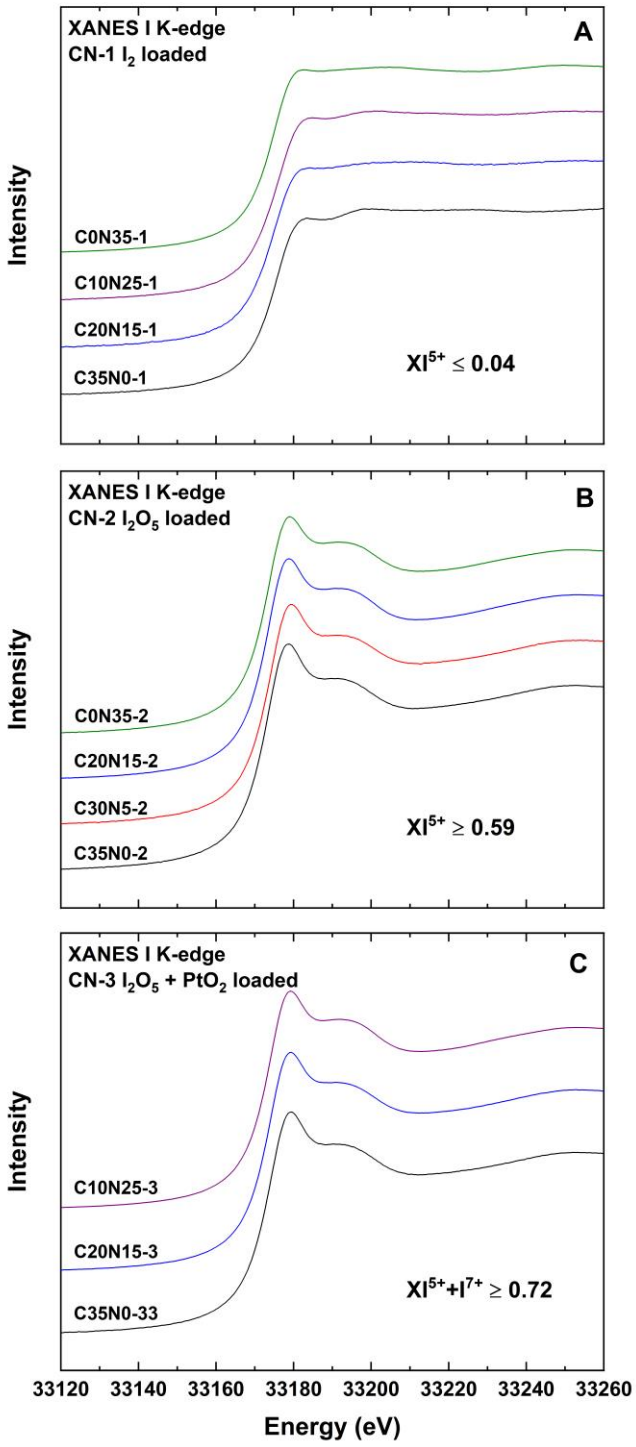

600

601 Figure 2

602

603

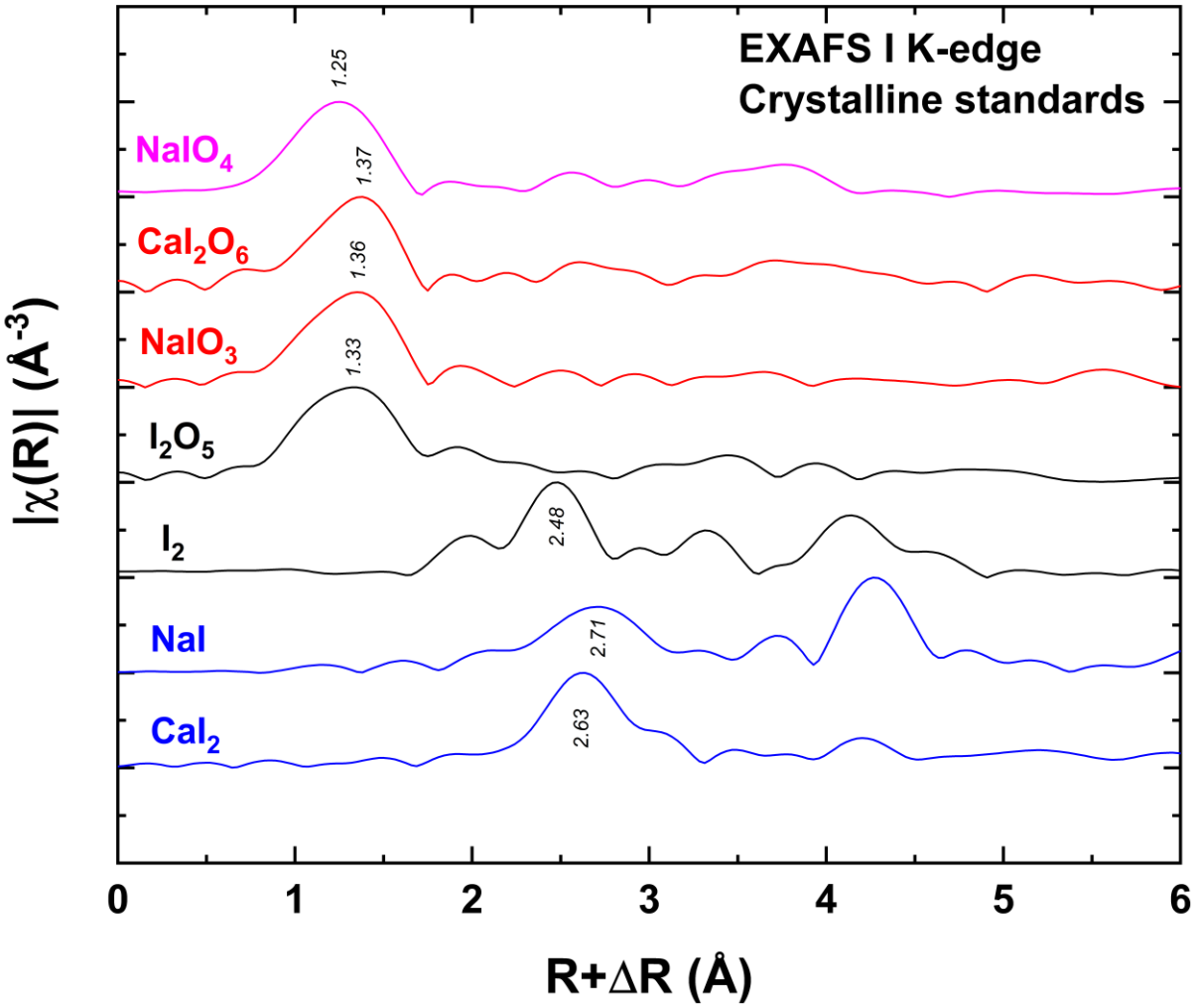

604

605 Figure 3

606

607

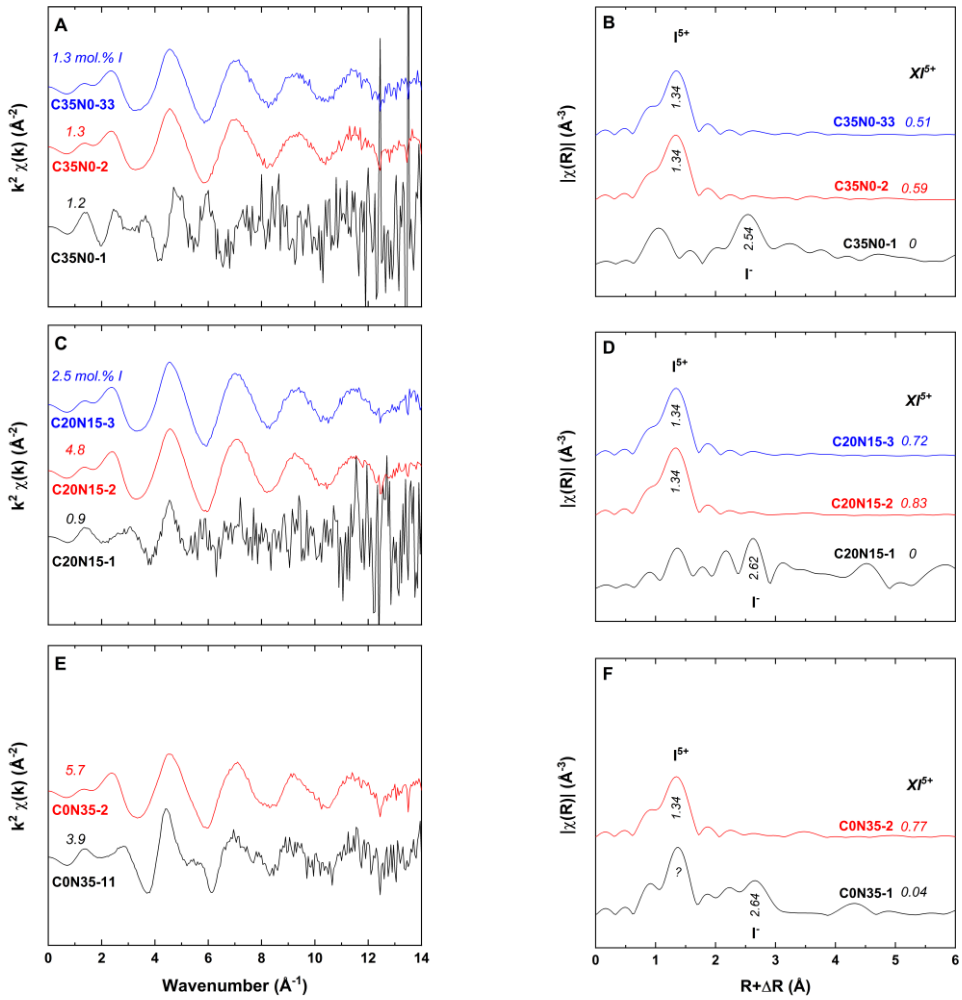

608

609 Figure 4

610

611

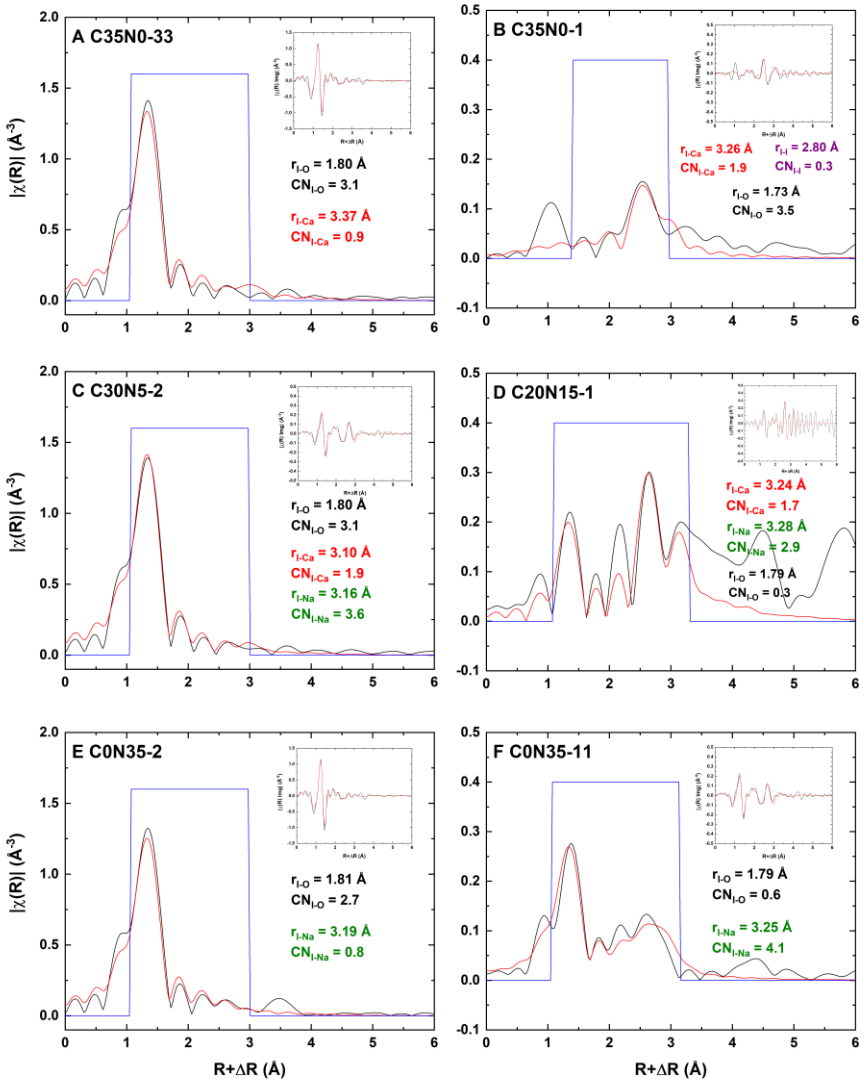

612

613 Figure 5

614

615

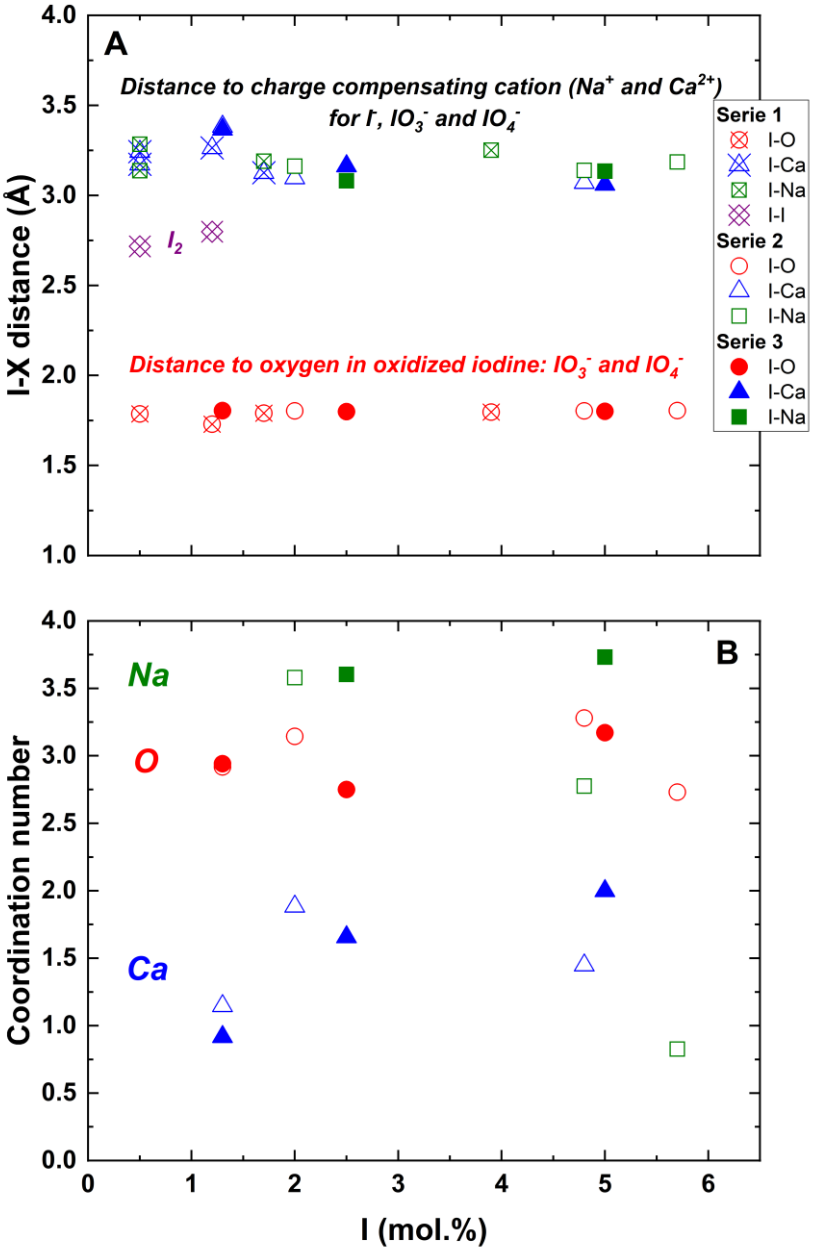

616

617 Figure 6

618

619

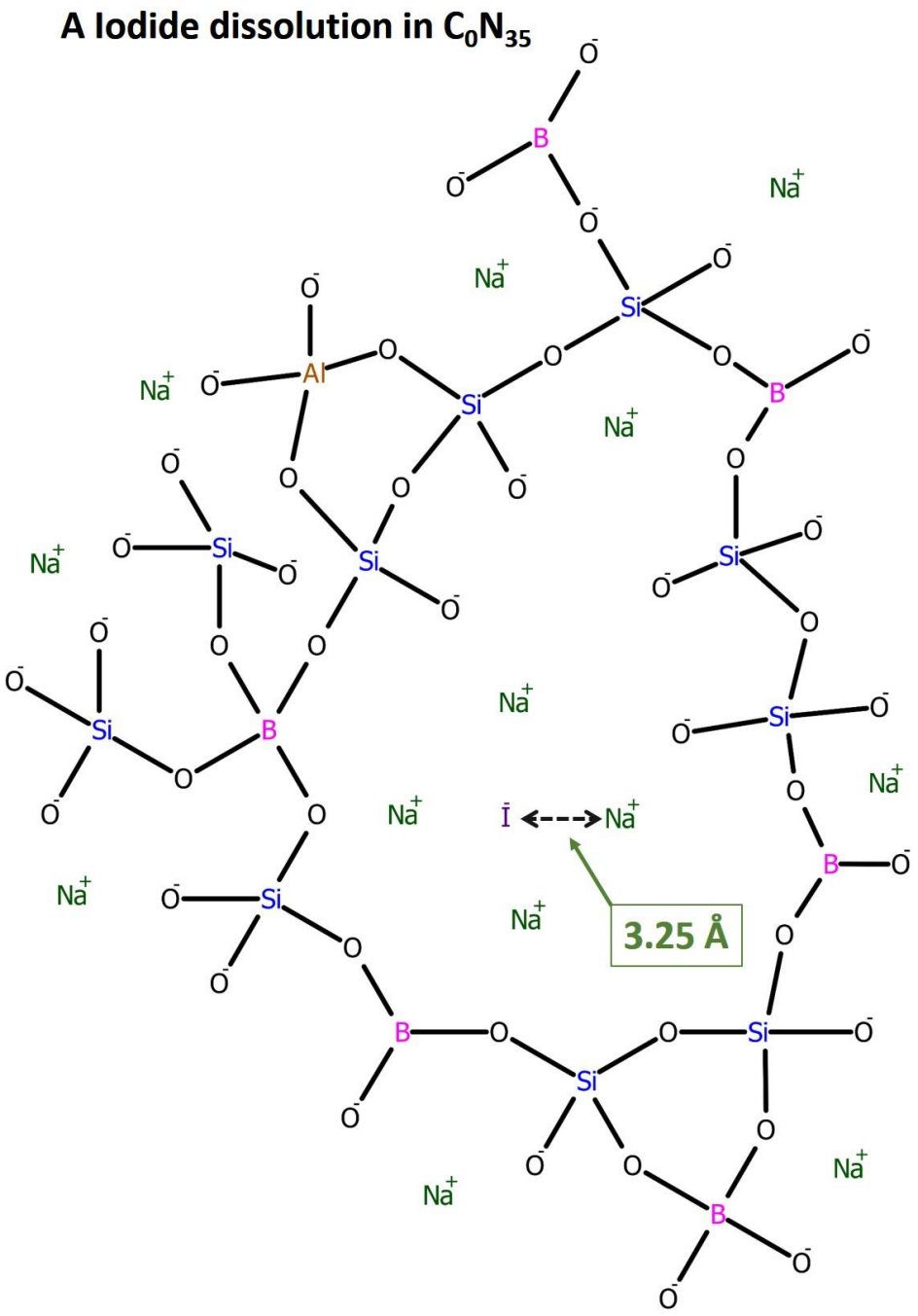

620

621 Figure 7A

622

623

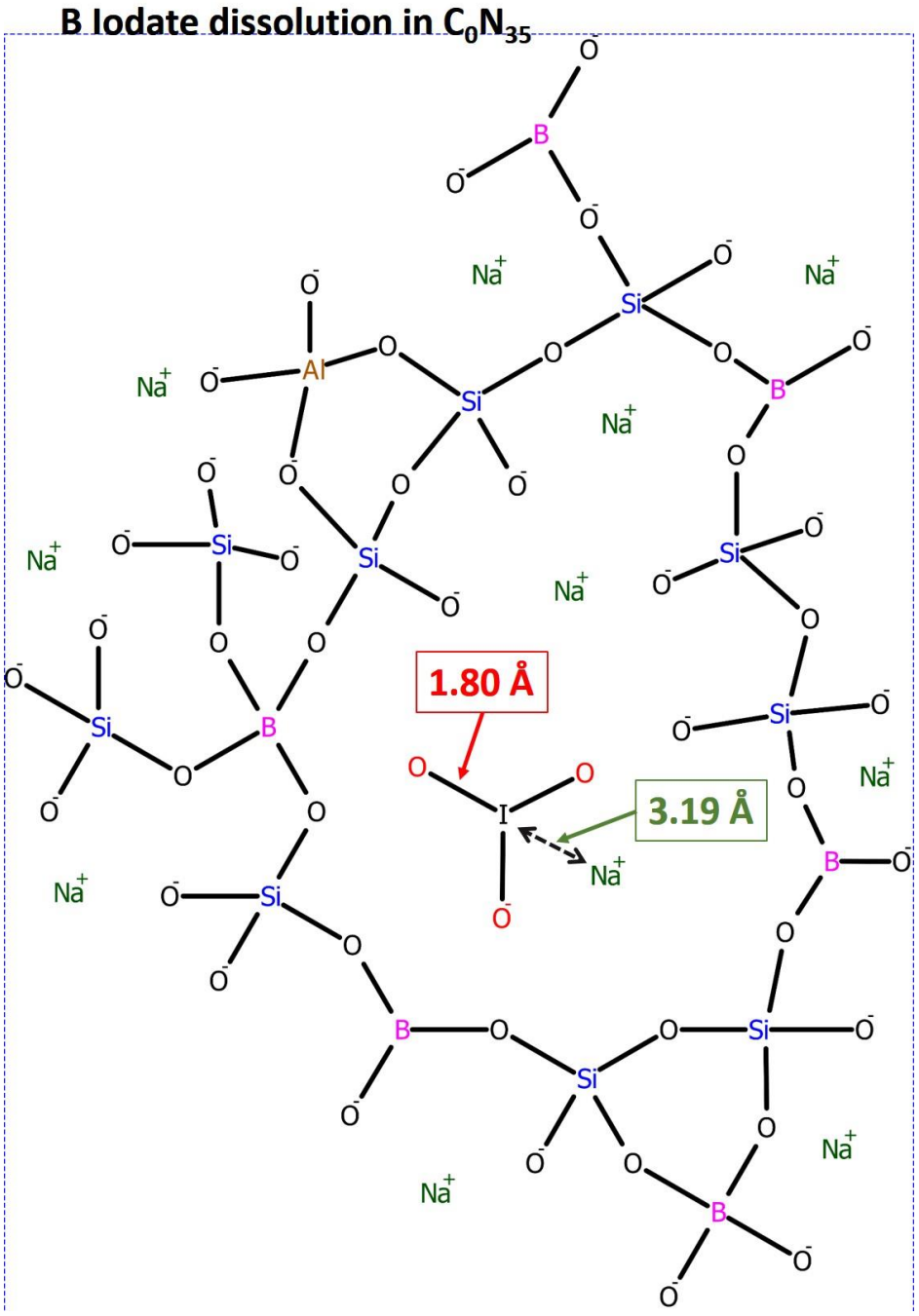

624

625 Figure 7B

626